Yiyuan Tu [1a]

Zhiduo Zhang[b]

Xiaoyu Cai[c]

Jiasi Wei[c]

Guoqing Ding [a*]

Multifactorial Discrepancies in the Spatiotemporal Driving Mechanisms of Urban Ecological Quality: Evidence from Shanghai, China

Journal of Electrical Systems

Abstract: - Urban ecological quality (UEQ) suffers from dramatic changes due to influence factors from multiple sources such as intensified human activity and climate change. A comprehensive analysis of the driving mechanisms is imperative for targeted ecological management. However, existing studies lack a spatiotemporal perspective to explore the discrepancies in driving mechanisms among multiple factors in detail. To address this critical gap, we established a spatiotemporal sequence of remote sensing ecological index (RSEI) from 2000 to 2020 in Shanghai and employed Geographically and Temporally Weighted Regression (GTWR) to meticulously investigate the multiple driving factors. Additionally, we utilized the K-Means clustering to uncover differentiation in the driving characteristics and mechanisms among different factors. Our findings revealed profound insights: 1) The overall RSEI exhibited a marginal decline from 2000 to 2005, followed by an improvement from 2005 to 2020 in Shanghai. The UEQ was mainly driven by the vegetation communities and also influenced and disturbed by a combination of abiotic factors including human activities, climate, soil, and topography. 2) The clustering of UEQ evolution in Shanghai is consistent with a certain urban-rural gradient. Multiple factors' driving roles and characteristics differ in distinct clustering areas, forming differentiated driving mechanisms that jointly influence the trajectory of UEQ spatiotemporal evolution. 3) Human activities play the largest negative inhibitory role among all drivers. Climatic factors show highly fluctuating time serial characteristics. This case study taking Shanghai as an example, not only depicts the evolutionary trajectory of UEQ in the last two decades but also analyzes and reveals in detail multifactorial discrepancies in the spatiotemporal driving mechanisms. Our research can provide references for environmental observations, targeted ecological management, and planning in Shanghai and other urban areas.

Keywords: Remote sensing ecological index; Geographically and temporally weighted regression; Multi-factor; K-Means; Shanghai

1 INTRODUCTION

Ecological quality represents the inherent capacity of diverse interconnected environmental components to support human survival and facilitate sustainable development, comprehensively encapsulating the regional

[1] * Correspondence: gqding0@sjtu.edu.cn; Tel.: +86-186-1633-0527

[a] School of Electronic Information and Electrical Engineering ,Shanghai Jiao Tong University, Shanghai, 201100,China;

[b] School of Design & China Institute for Urban Governance, Shanghai Jiao Tong University, Shanghai 200240, China

[c] Key Laboratory of Bioanalysis and Metrology for State Market Regulation, Shanghai Institute of Measurement and Testing Technology, No. 1500 Zhangheng Road, Shanghai 201203, China

Emails: 446074397@sjtu.edu.cn (Y.T.); zhangzhiduo12532255@sjtu.edu.cn (Z.Z.); caixiaoyu@simt.com.cn (X.C.); weijs@simt.com.cn (J.W.); gqding0@sjtu.edu.cn (G.D.)

Copyright © JES 2024 on-line : journal.esrgroups.org

holistic ecological state (Chen and Yang et al., 2022). Over 56.5% of the world's population resides in urban areas (https://databank.worldbank.org) today, and the swelling population is responsible for an ever-increasing ecological burden (Khan and Hou et al., 2021). Urban ecological quality (UEQ) also suffers from more acute multi-source ecological risks (Arfanuzzaman and Dahiya, 2019), including climate change (Wang and Fu et al., 2023) and soil degradation (Toth and Dombos et al., 2023). Facing the urgent issue of enhancing ecosystem services and advancing human well-being for sustainable development (Knight and McClean et al., 2022), the United Nations has emphasized the need for a multi-level and comprehensive assessment of global ecosystems through initiatives such as the Sustainable Development Goals for 2030 (SDGs) and the Millennium Ecosystem Assessment Program (Komugabe-Dixson and de Ville et al., 2019). Therefore, a spatiotemporal investigation of the driving mechanisms of UEQ (Li and Wang, 2022), is one of the guarantees for identifying ecological problems and causes as well as developing appropriate adaptive mitigation strategies (Zhang and Yang et al., 2021), which is the departure point of the study.

Researchers have devised various indices or frameworks to quantify UEQ, but not all of them reveal its spatiotemporal heterogeneity sufficiently at the regional scale. Evaluation frameworks incorporating economic and social variables with the coarse spatial resolution are generally appropriate only for macro-scale studies, examples including the ecological footprint (EFP) estimated through the STIRPAT model (Dogan and Ulucak et al., 2020), and the coordination of urbanization and ecological environment composite system (CUECS) (Wang and Liang et al., 2019). Due to the benefits of sufficient datasets and spatiotemporal continuity, remote sensing has provided an effective approach to focus on the ecological environment in detail and studied how external factors affect UEQ. Comprehensive remote sensing indices have become a focus for most scholars, as single remote sensing indices can only one-sidedly reflect the state of the ecosystem. The remote sensing ecological index (RSEI) is an efficient and generalized measure in large-scale UEQ studies (Ji and Wang et al., 2020), compared with other UEQ assessment index systems (Tang and Liu et al., 2023). Some researchers proposed enhancements to RSEI (Jiang and Zhang et al., 2021; Zheng and Wu et al., 2022; Wang and Chen et al., 2023). There is still little empirical support for these improved models, and their availability and dependability are still in doubt (Xu and Li et al., 2022). Nonetheless, the original RSEI is a reliable, efficient, and widely-utilized method for identifying interannual UEQ changes in urban areas (Hu and Xu, 2018), river basins (Yuan and Fu et al., 2021), and nature reserves (Jing and Zhang et al., 2020).

Multiple dimensions including human activities (Frédéric and Jean-Marc, 2018), climate change (Braun and de Jong et al., 2019), soil quality (Arfanuzzaman and Dahiya, 2019), and topographic conditions (Geng and Yu et al., 2022), were considered as potential drivers of regional UEQ changes. In addition, excluding the growth of biotic communities after external disturbances, especially vegetation communities, has an irreplaceable function of improving UEQ. There are definite discrepancies in the driving mechanisms among different factors, mainly due to the spatiotemporal heterogeneity characteristics of the impacts (Wang and Liu et al., 2021), which has led researchers to recognize more rigorous standards when investigating driving mechanisms. Data requirements necessitate the collection of extensive and long-term datasets with high spatiotemporal resolutions (Sun and Li et al., 2022). Instead of constructing a continuous yearly or monthly series (Zhang and Fan et al., 2023), quantities of studies still rely on a limited number of samples at different time points (Zhang and Cai et al., 2022), which

overlooks the temporal variability of effects and can result in biased conclusions. The traditional driving factors regression models, such as ordinary least squares regression (OLS) and autoregressive integrated moving average (ARIMA) (Bo and Li et al., 2022), ignore the mutual influence of the spatial locations, while temporal requirements still cannot be met by spatial regression models like Geographically Weighted Regression (GWR) and Geographically Weighted Detector (Lyu and Clarke et al., 2019). To address this issue, models that consider spatiotemporal effects, such as the Geographical temporal weighted regression model (GTWR) (Zou and Zhu et al., 2022) and spatial Durbin models (Li and Bi et al., 2022), have become utilized in some studies of ecological drivers, with more reliable results compared to conventional models.

Furthermore, the spatiotemporal heterogeneity of both UEQ and driver influences tends to produce massive pixel samples, complicating the analysis of the driving mechanisms. From a spatiotemporal perspective, each pixel corresponds to a time series, and appropriate clustering can reflect the spatial difference distribution of evolution (Suominen, 2018). Some studies use the increase/decrease and trend significance (Xu and Wang et al., 2019) to divide time series, emphasizing trend characteristics while ignoring other features such as contour and fluctuation. Another popular categorization and partitioning methods are the autocorrelation indices. But examples like the Global Moran's I, the Anselin Local Moran's I (Ren and Shang et al., 2020), and the local hotspots Getis-Ord Gi* cannot fully capture the changes in the temporal dimension. Most of the existing studies are limited to the above schemes and are inaccessible to delve into the spatiotemporal differences between the driving mechanisms of multiple factors. For the above challenges, machine learning has been providing effective means for time series clustering, offering more suitable solutions for the various time series features. Dynamic time warping (DTW) and K-Means clustering (Viana-Soto and Aguado et al., 2020) are proven valid as machine learning techniques for time series clustering in ecological index research. By applying the K-Means, we can take into account both the contour and trend characteristics of the UEQ time series and avoid getting one-sided clustering results for driving pattern and mechanism analysis betterment.

Based on the foregoing context, we pose the following significant scientific query: *What are the discrepancies in the spatiotemporal driving mechanisms on UEQ from multi-factor, and how do reveal them?* To address this issue, we selected Shanghai, a prototypical megacity that has undergone tremendous changes in UEQ and drivers during its rapid development and construction, as the typical research region. This study aims to explore the dynamics of Shanghai UEQ and drivers, dig deeper into the discrepancies in driving mechanisms of different factors, and summarize the possible universal patterns. This study will offer a reference for revealing the driving patterns of multiple factors on UEQ from a spatiotemporal perspective, provide a solid research foundation for targeted ecosystem management, and have potential significance for regional sustainable development.

2 MATERIALS AND METHODS

2.1 Study area

Shanghai (120°51′09″-121°58′17″E, 30°41′28″-31°51′56″N) is a megacity located in the coastal region of China and the Yangtze River Delta, on the west coast of the Pacific Ocean, and at the east end of the Asian continent, as shown in Figure 1(a). The region has an approximate area of 6,791.41 km^2. Shanghai is characterized by flat terrain with an average slope of 1.1° and an average elevation of 4.1 m above sea level

(https://tjj.sh.gov.cn/zrdl/index.html). The region has a subtropical monsoon climate, which results in hot, humid summers and cool, damp winters. The average annual precipitation and temperature are approximately 1,166.1 mm and 16.0°C, respectively (https://data.cma.cn/). Over the past two decades, the urban area in Shanghai has experienced significant expansion, with impervious surface area, total population, and GDP continuing to increase, as shown in Figures 1(b), 1(c), and 1(d), indicating the regional ongoing urbanization and increasing human activities. As of 2021, the population of Shanghai has reached about 24.89 million, ranking it as the third-largest city in the world. The regional gross domestic product (GDP) in 2021 was 4,321.49 billion yuan (https://tjj.sh.gov.cn/). Construction land (42.69%) and cropland (41.50%) dominate the current land use/cover in Shanghai, as depicted in Figure 1(e), severely limiting the spatial scope of natural ecological systems such as forests and challenging the regional environment.

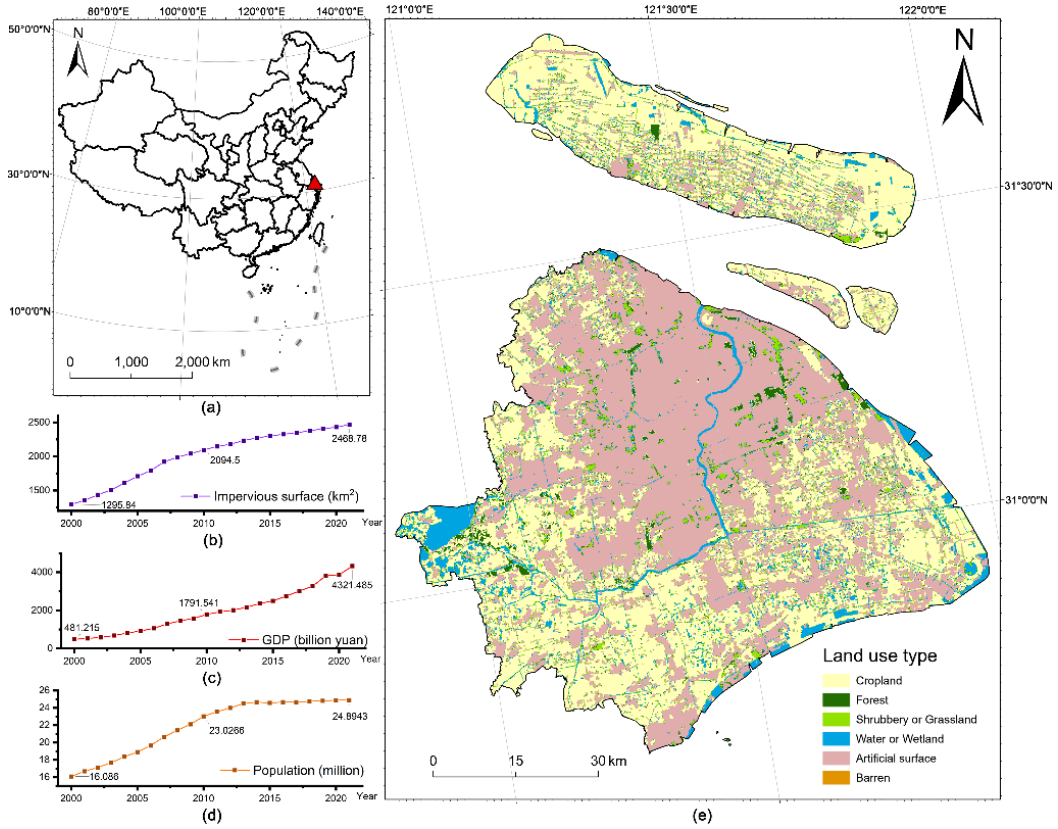

Fig 1. (a) Shanghai location map; (b) Shanghai impervious surface area curve from 2000-2021; (c) Shanghai population curve from 2000-2021; (d) Shanghai GDP curve from 2000-2021; (e) Shanghai land use cover map in 2020

2.2 Data source and processing

The research process consists of several stages, including data collection and variable calculation, variable integration, time series clustering, and driving analysis. A detailed overview of the research process is depicted in Figure 2.

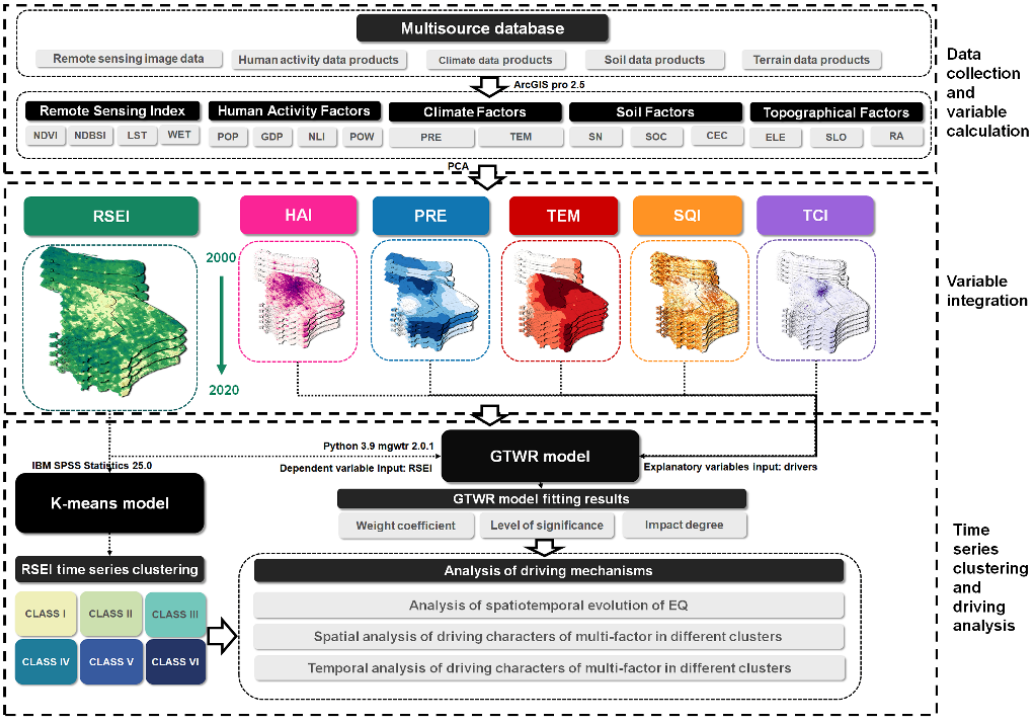

Fig 2. Technical flowchart of the methodology

In this study, Table A1 presents the data sources and variables used. The 2021 Shanghai administrative boundary shapefile was employed to identify the study area. The Landsat Collection 2 dataset from the United States Geological Survey (USGS) provided by Google Earth Engine (GEE) was used to obtain surface reflectance data for 2000-2011 and 2013-2020, using corrected Landsat 5 TM and Landsat 8 OLI imagery, respectively. The growing season (June to September) of each year was selected to calculate the RSEI (Yang and Tian et al., 2021) while missing data for 2012 were estimated through temporal interpolation from neighboring years. We employed the GEE-provided cloud removal algorithm to remove clouds and shadows, based on QA_PIXEL (Li and Wang, 2022), and calculated the median to synthesize high-quality multi-band images. Besides, we referred to other research results and numerous widely accepted data products as the foundation for extracting drivers. Population data came from WorldPop (https://www.worldpop.org/); GDP data (Chen and Gao et al., 2022), nighttime lights (Chen and Yu et al., 2021), and land use data (Yang and Huang, 2021) came from open-source research of other scholars. The land use data was validated by visual interpretation of high-resolution images from Google Earth (http://www.google.com/earth) and has a classification accuracy of over 85% for Shanghai, which meets the research needs. Other sources such as Terrain data from NASA DEM developed by SRTM imagery (https://lpdaac.usgs.gov/products/nasadem_hgtv001/), climate data from the CRU Ts4.0 (Harris and Osborn et al., 2020), and soil data from the SoilGrids (Poggio and de Sousa et al., 2021) were also used as references.

Table A2 illustrates the data processing procedures and calculations that yielded five categories of 16 distinctive variables. The remote sensing ecological indices used to describe the UEQ consist of the normalized difference vegetation index (NDVI), normalized difference build-up and soil index (NDBSI), land surface temperature (LST), and wetness index (WET). These indices were obtained from remote sensing image data by employing specific methods detailed in section 2.3.1. Human activity factors, including population density (POP), GDP density

(GDP), nighttime light (NL), and land use intensity (LUI), were incorporated into the analysis (Cheng and Liu et al., 2022). The climate variables, precipitation (PRE), and temperature (TEM) were computed from the total precipitation amount and the average temperature in Shanghai from June to September. The terrain variables include commonly used elevation (ELE), slope (SLO), and relief amplitude (RA). The soil variables considered were soil organic content (SOC), nitrogen (SN), and cation exchange capacity (CEC), which are widely accepted as indicators of soil fertility and quality (Paul and Saha et al., 2020). Although other variables showed annual variations, the terrain and soil data exhibited relatively little variation in site conditions, and thus single-year data were used. All variables underwent processing using ArcGIS Pro 2.5 geoprocessing, resampling, or spatial interpolation to maintain a consistent spatial resolution of 100m × 100m and were extracted by the study area boundary mask. The variance inflation factor (VIF) was used to detect multicollinearity among the variables, and it was observed that NL (7.530), GDP (9.340), SLO (9.329), and RA (9.163) had higher VIF values (>7.5), indicating significant collinearity issues. Thus, dimensionality reduction processing of the variables was necessary, as stated in section 2.3.2.

2.3 Methods

2.3.1 Remote sensing ecological index (RSEI) calculation

Greenness, dryness, heat, and wetness are the four univariate indices that make up the RSEI. The greenness index is a crucial metric to reflect the development and coverage of vegetation. NDVI, the most widely used greenness index, is calculated as Equation (1):

$$NDVI = \frac{\rho_{nir} - \rho_{red}}{\rho_{nir} + \rho_{red}} \tag{1}$$

Where: ρ_{nir} and ρ_{red} represent the reflectance in the near-infrared and red bands of the image, respectively. NDBSI is synthesized using the Index-based Built-up Index (IBI) and the Soil index (SI) with equal weights, calculated as shown in Equation (2):

$$NDBSI = \left(SI + IBI\right)/2 \tag{2}$$

Where: IBI represents the degree of imperviousness of the ground surface, indicating the density of buildings and hard surfaces, and is calculated as shown in Equation (3). SI reflects the degree of bare ground and land degradation, calculated as shown in Equation (4).

$$IBI = \frac{2\rho_{swir2}/\left(\rho_{swr1} + \rho_{nir}\right) - \left[\rho_{nir}/\left(\rho_{red} + \rho_{nir}\right) + \rho_{green}/\left(\rho_{swir1} + \rho_{green}\right)\right]}{2\rho_{swir2}/\left(\rho_{swr1} + \rho_{nir}\right) + \left[\rho_{nir}/\left(\rho_{red} + \rho_{nir}\right) + \rho_{green}/\left(\rho_{swir1} + \rho_{green}\right)\right]} \tag{3}$$

$$SI = \frac{\left(\rho_{swir1} + \rho_{red}\right) - \left(\rho_{blue} + \rho_{nir}\right)}{\left(\rho_{swir1} + \rho_{red}\right) + \left(\rho_{blue} + \rho_{nir}\right)} \tag{4}$$

Where: ρ_{blue}, ρ_{green}, ρ_{red}, ρ_{nir}, ρ_{swir1}, ρ_{swir2} indicate the reflectance of features in the blue, green, red,

near-infrared, short-wave infrared1, and short-wave infrared2 bands corresponding to the images, respectively. Applying a specific emissivity correction to the sensor temperature measurements results in the calculation of the Land Surface Temperature (LST) characterization heat index using remote sensing inversion (Guo and Fang et al., 2020). Its formula is shown in Equation (5).

$$LST = \frac{T}{1+\left(\frac{\lambda T}{\rho}\right)\times \ln \varepsilon} \tag{5}$$

Where: λ is the central wavelength of thermal IR 6-band and 10-band, 11.435 μm, and 10.896 μm for both TM and OLI images, respectively; ρ is an adjustment factor with a value of 1.438×10^{-2}mk; ε is the surface radiance, calculated according to the literature (Nichol, 2005). T is the sensor temperature value, which is calculated from the thermal IR 6-band and 10-band image elements at the radiation value L_λ at the sensor. The formulas of T and L_λ are shown in Equations (6) and (7), respectively.

$$T = \frac{K_2}{\ln\left(\frac{K_1}{L_\lambda}+1\right)} \tag{6}$$

$$L_\lambda = gain\times DN + bias \tag{7}$$

Where: the calibration parameters K_1=606.09W/(m^2·sr·μm), K_2=1282.71K, DN is the grayscale number of the image element, and $gain$ and $bias$ are the gain and bias values of the corresponding band, respectively (Nichol, 2005). The WET calculation based on Landsat 5 TM and Landsat 8 OLI remote sensing data are shown in Equations (8) and (9), respectively (Ariken and Zhang et al., 2020).

$$WET(TM)=0.0315\rho_{blue}+0.0201\rho_{green}+0.3102\rho_{red}+0.1594\rho_{nir}-0.6806\rho_{swir1}-0.6109\rho_{swir2} \tag{8}$$

$$WET(OLI)=0.1511\rho_{blue}+0.1973\rho_{green}+0.3283\rho_{red}+0.3407\rho_{nir}-0.7117\rho_{swir1}-0.4559\rho_{swir2} \tag{9}$$

Where: ρ_{blue}, ρ_{green}, ρ_{red}, ρ_{nir}, ρ_{swir1}, ρ_{swir2} are the wavelength reflectance of blue, green, red, NIR, SWIR1, and SWIR2, respectively.

2.3.2 Principal component analysis (PCA)

We built several composite indices using PCA: the RSEI for ecological quality, the HAI for human activity intensity, the SQI for soil quality, and the TCI for topographic conditions. Through linear transformation and sequential vertical axes rotation, PCA reduces the number of components that make up information on multiple variables. To avoid the weight imbalance, probably from the non-uniformity of the magnitudes, the variable factors should be studentized before PCA, as Equation (10) shows.

$$NI_i = \left(I_i - I_{\min}\right)/\left(I_{\max} - I_{\min}\right) \tag{10}$$

Where: N_i is the studentized result of the ith pixel of a variable; $I_i$is the variable value at the ith pixel; I_{max} is the maximum value of the variable among all pixels; I_{min} is the minimum value of the variable among all pixels. Equations (11-14) show the composite indices constructed by PCA.

$$RSEI_i = PCA\left[f\left(NDVI, NDBSI, LST, WET\right)\right] \quad (11)$$

$$HAI_i = PCA\left[f\left(GDP, POP, NL, POW\right)\right] \quad (12)$$

$$SQI_i = PCA\left[f\left(SOC, SN, CEC\right)\right] \quad (13)$$

$$TCI_i = PCA\left[f\left(ELE, SLO, RA\right)\right] \quad (14)$$

As shown in Table A3, all four composite indices passed the Kaiser-Meyer-Olkin (KMO) test (KMO>0.6, p<0.001), and the eigenvalue load shares of the first principal component exceeded 70%, proving the applicability and suitability of PCA. In addition, PRE and TEM had low correlations and failed the test to extract a valid single maximum principal component, so they were considered separately as driver variables. For comparability, the indices were further studentized through Eqs. (8). Subsequently, we tested the covariance of the variables, and the VIF values of the driver variables were calculated as HAI (2.509), PRE (1.111), TEM (1.436), SQI (1.787), and TCI (1.417), all of which met the requirement of <7.5, indicating no significant covariance between the variables.

2.3.3 Geographical temporal weighted regression (GTWR) model

GTWR is an extension of GWR that addresses the non-smoothness in parameter estimation caused by spatiotemporal distance. The weight matrix utilized in GTWR is developed by taking into account the differences in spatiotemporal data, which allows for a more flexible and comprehensive analysis of complex spatiotemporal data (Hu and Zhang et al., 2022). The GTWR model expression is shown in Equation (15) (Huang and Wu et al., 2010).

$$Y_i = \beta_0\left(u_i, v_i, t_i\right) + \sum_{k=1}^{p} \beta_k\left(u_i, v_i, t_i\right) X_{ik} + \varepsilon_i \quad (15)$$

Where: Y_i is the dependent variable of the ith spatiotemporal sample, which is the RSEI value in this study; X_{ik} is the kth explanatory variable of the ith sample. p is the total number of explanatory variables, and a total of five explanatory variables, HAI, PRE, TEM, SQI, and TCI, are considered in this study. u_i, v_i, and t_i denote the longitude, latitude, and time coordinate of the ith sample, respectively. $\beta_0(u_i, v_i, t_i)$ is the spatial and temporal intercept of the sample, which indicates that the original vegetation community of the ecosystem grows potentially with capacity on its own, eliminating outside interference. $\beta_k(u_i, v_i, t_i)$ passes through the regression coefficient of the kth variable of the ith sample. ε_i represents the independent random error term, which follows a normal distribution of $N(0, \delta^2)$. Then we calculated the estimates of the regression coefficients $\hat{\beta}(u_i, v_i, t_i)$ using the locally weighted least squares method with the formula shown in Equation (16).

$$\hat{\beta}(u_i, v_i, t_i) = \left(X^T W(u_i, v_i, t_i) X\right)^{-1} X^T W(u_i, v_i, t_i) Y \quad (16)$$

Where: X is the matrix of explanatory variables; Y is the vector of dependent variables. $W(u_i, v_i, t_i)$ is the diagonal matrix of spatiotemporal distance weights, and matrix element ω_{ij} is the spatiotemporal weight between sample i and j, estimated using a Gaussian kernel function under adaptive bandwidth, as shown in Equation (17).

$$\omega_{ij} = \exp\left[-\frac{\left(d_{ij}^{ST}\right)^2}{h_{ST}^2}\right] \quad (17)$$

Where: d_{ij}^{ST} is the spatiotemporal distance between sample i and j, and h_{ST} is the spatiotemporal bandwidth. The measure of spatiotemporal distance combines temporal and spatial distances and is expressed as a linear combination of the two, as shown in Equation (18).

$$d_{ij}^{ST} = \lambda d_{ij}^{S} + \mu d_{ij}^{T} \quad (18)$$

Where: d_{ij}^{S} and d_{ij}^{T} are the spatial and temporal distance between sample i and j, respectively; λ and μ are the corresponding weights. In GTWR, h_{ST}, λ, and μ are the hyperparameters to be tuned. To find the ideal set of hyperparameters, we employed CV cross-validation (Cheng and Dai et al., 2016). We diagnosed the model using several valid statistics (Wei and Zhang et al., 2019), and Table A4 shows the detailed results. With lower AICc, RMSE, and Global Moran' I than OLS and GWR and the greatest Adjusted R2, GTWR is the best match for our data in this study and is more appropriate for driver analysis.

2.3.4 K-Means for time series clustering

As a commonly used unsupervised learning clustering algorithm, K-Means works by iteratively optimizing a partitioning scheme of K clusters, such that the loss function corresponding to the clustering result is minimized (Kun and Zhenyu et al., 2019). By leveraging a multitude of time series attributes, K-Means clustering enables comprehensive and nuanced clustering analysis, addressing the shortcomings of traditional clustering methods that are limited to a smaller number of characteristics (Yu and Shao et al., 2018). In order to investigate the patterns and underlying factors driving changes in the UEQ, we utilized this method to classify the RSEI time series data.

Following the standard procedures of K-Means clustering, this research executed data preprocessing on the calculated RSEI, including the procedures of filtering for normalization and outliers to ensure the reliability of the subsequent analysis. With the assistance of IBM SPSS Statistics 25.0, this study randomly allocated the initial cluster centers and defined the loss function $J(c, \mu)$ as the sum of squares of the distances of each sample from the cluster centroids to which it belonged, as shown in Equation (19).

$$J(c, \mu) = \sum_{i=1}^{M} \left\| x_i - \mu_{c_i} \right\|^2 \quad (19)$$

Where: x_i represents the ith sample belonging to cluster c_i; μ_{ci} denotes the cluster centroid; M is the

total sample size. Iterative reassignment of sample categories and recalculation of category clustering centers are key procedures in K-Means clustering until the loss function converges and successful clustering is achieved. An important hyperparameter of this model is the number of clusters, denoted by K, which is typically fine-tuned by a reference test to determine the elbow point of the sum of error squares (SEE) curve, indicating the ideal value (Wang and Ma et al., 2019). The SEE-K curve for the RSEI time series is depicted in Figure A1, revealing that the payoff of the degree of aggregation gained by increasing K diminishes rapidly. Therefore, for this study, K = 6 is deemed a suitable choice because the elbow of the curve indicates that the number of clusters is adequate to maintain SEE at a low level.

3 RESULTS

3.1 RSEI evolution and time series clustering in Shanghai

The RSEI temporal change in Shanghai was examined, as presented in Figure 3. The overall RSEI demonstrated an upward fluctuation from 2000 to 2020, indicating a gradual improvement in the UEQ during the previous two decades. Notably, the RSEI reached its lowest point of 0.410 in 2005 and its highest position of 0.579 in 2020. The temporal change in a frequency distribution is evident from histogram Figures 3(b-e). A decrease in the region with RSEI between 0.45 and 0.60 and a considerable increase between 0.20 and 0.45 are responsible for the minor deterioration in UEQ between 2000 and 2005. Between 2010 and 2015, the area with RSEI below 0.30 decreased, and between 2015 and 2020, the area above 0.60 significantly increased with a rightward shift in the frequency histogram from 2005 to 2020, indicating a definite enhancing trend of UEQ.

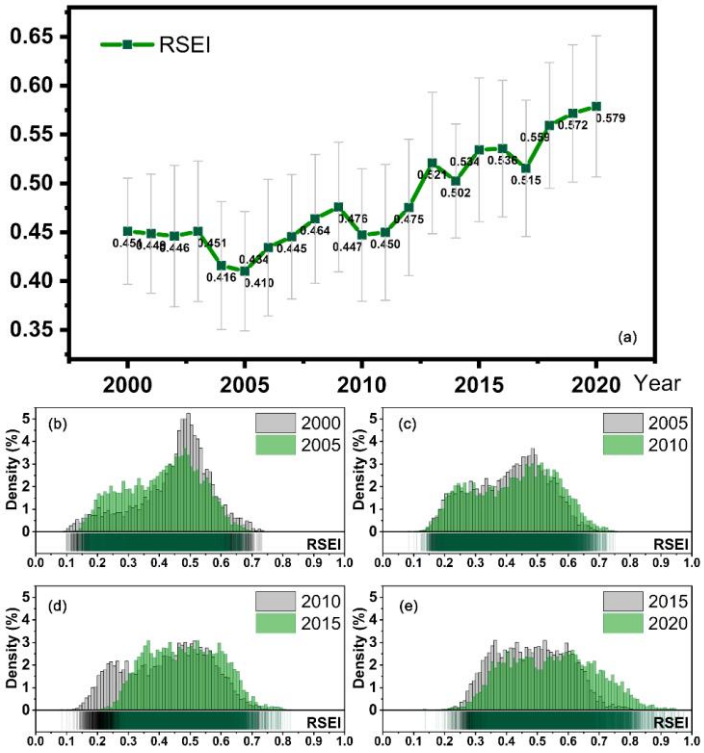

Fig 3. Overall temporal changes of RSEI in Shanghai: (a) RSEI time series curve from 2000 to 2020; Comparison Chart of RSEI Frequency Distribution: (b) 2000 and 2005 (c) 2005 and 2010 (d) 2010 and 2015 (e) 2015 and 2020

The spatial distribution of RSEI across Shanghai for various years was analyzed and presented in Figure 4. The northern and western parts of Shanghai, including Chongming Island, experienced a decline in RSEI levels between 2000 and 2005, while low RSEI areas expanded. In contrast, from 2005 to 2020, low RSEI locations decreased, and the southwest and other southern regions of Shanghai witnessed progressive improvements in RSEI levels. This spatial trend is consistent with the time-series pattern observed in Figure 3, indicating an overall UEQ improvement tendency. Specifically, the western side of Chongming Island, the Chongming East Beach region, and the southwest portion of Shanghai exhibited high RSEI levels, whereas the urbanized core region of Shanghai had a low or relatively low RSEI up to 2020.

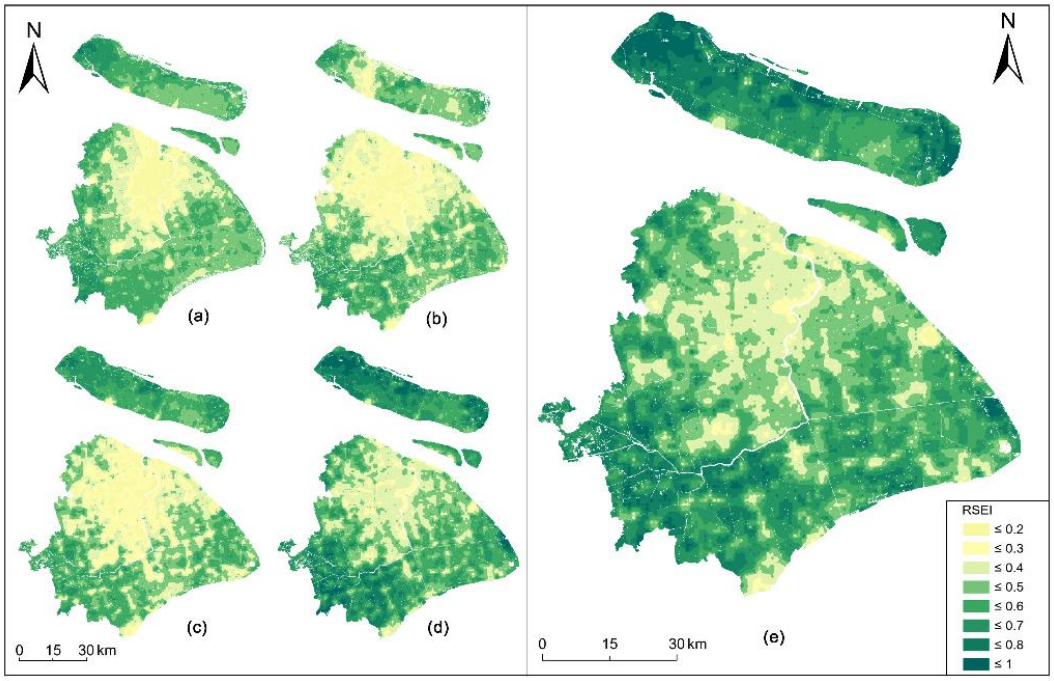

Fig.4 Spatial distribution map of Shanghai RSEI in different years: (a) 2000; (b) 2005; (c) 2010; (d) 2015; (e) 2020

The spatiotemporal distribution of RSEI was examined using time-series clustering analysis, resulting in the formation of six distinct clusters, as depicted in Figure 5(a). The proportions and areas of each clustering category are shown in Figure 5(b), while Figure 5(c) displays the time series of RSEI for each class. The results of this analysis demonstrate significant urban-rural disparities in the spatial distribution of clusters, suggesting that UEQ change patterns may differ depending on the urban-rural gradient. The spatial distribution of RSEI and its time series reveal an upward trend from the city center to the suburbs and subsequently to the townships in the contouring features. Regarding trend characteristics, Classes I, IV, V, and VI all displayed a highly significant linear increasing trend ($p<0.001$, $n=21$), while Classes II and III did not exhibit a significant linear increasing trend (Class II, $p=0.027$, $n=21$; Class III, $p=0.004$, $n=21$). Class II and III were located on the periphery of the core urban area and the peri-urban, respectively, and showed an overall trend of decreasing before increasing.

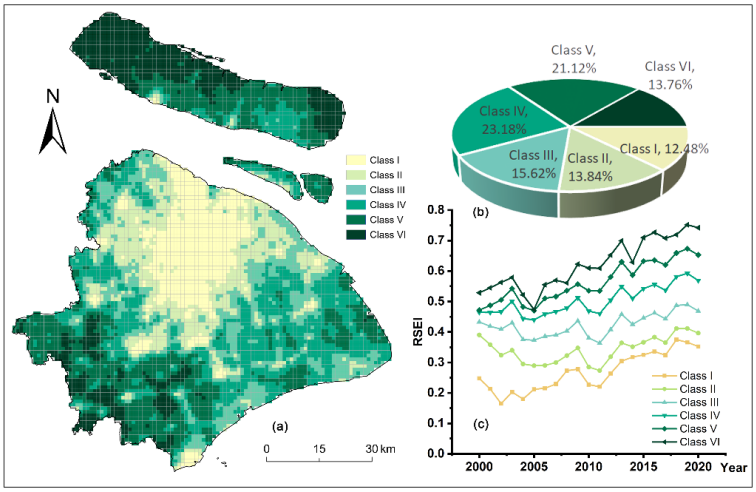

Fig 5. (a) Spatial distribution map of time series classes; (b) Area proportion of different classes; (c) RSEI time series change curve of different classes

3.2 Spatial analysis of multifactorial driving mechanisms

In Figure 6, the spatial distribution of the multi-year average impact values of the drivers is displayed. The analysis reveals that HAI exerts a widespread negative impact on most regions of Shanghai, with relatively severe effects observed in the densely built-up areas and more minor negative effects in the suburbs. In contrast, PRE has a more prominent positive influence on the coastal region, while TEM was found to be more positively influential in the suburbs. SQI positively affects most areas, but areas with dense impervious surfaces receive a very limited boost. The TCI impacts varied widely between regions and are detrimental to the light-colored, showing that the terrain conditions in some areas hinder the enhancement of the UEQ. The spatial distribution of intercept values shows the difference in the ability of biological or vegetation communities to improve themselves, with the western and eastern suburbs of Shanghai and Chongming Island in better condition.

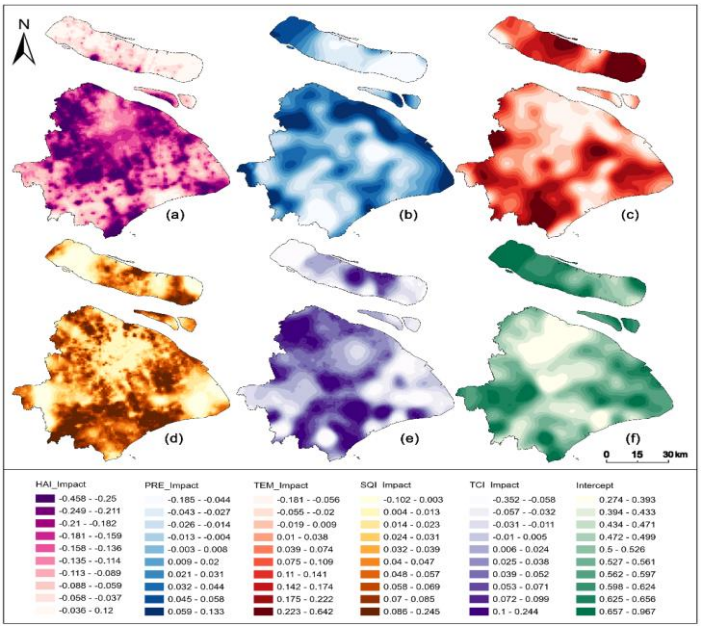

Fig 6. Spatial distribution of the multi-year average impact of drivers: (a) HAI; (b) PRE; (c) TEM; (d) SQI; (e) TCI; (f) Intercept

The partition statistics of the impact values of each driver according to clustering are shown in Figure 7. In all clusters, HAI showed inhibitory effects, with the strongest in Classes I, II, and III. The facilitation effect of PRE decreases the gradient of clustering change. TEM shows some negative effects in Class I, but a positive effect in other clusters, especially in Classes V and VI. SQI produces varying degrees of positive impact. Also of interest is the fact that TCI is the only one that plays a negative role in Class VI. In contrast to the biotic community components characterized by Intercept, the combined effect of multiple factors can be considered as a perturbation of abiotic components. Where this effect shows a slight inhibitory effect in Classes I-IV, a slight facilitative effect in Class V, and an insignificant effect in Class VI.

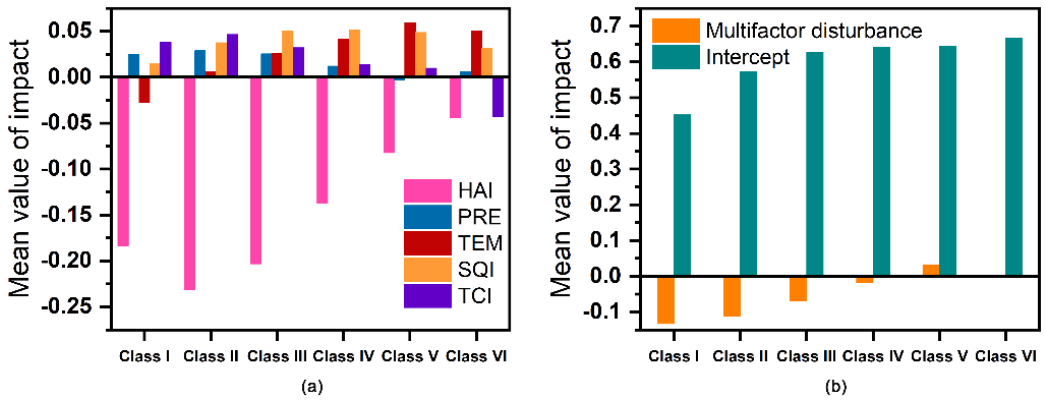

Fig 7. The mean value of driver impacts of clusters: (a) Comparison of factors; (b) Multifactor and intercept

To verify the reliability of the clustering statistics, we further examined the driving effects of the multiple factors on all samples. It can be seen in Figure A2(a) that the proportion of samples promoted or inhibited shows that HAI had an inhibitory effect on RSEI in 98.46% of spatiotemporal locations; SQI had a promoting effect on RSEI in 89.78% of spatiotemporal positions. However, not every factor had an impact weight that was statistically significant over the entire region. As shown in Figure A2(b), PRE, TEM, SQI, and TCI had no significant effects on 25.83%, 25.76%, 20.49%, and 42.68% of the areas, respectively ($|t|<1.960$, $p>0.05$, $n=14261625$).

3.3 Temporal analysis of multifactorial driving mechanisms

Figure 8(a) shows the change in the average weight values of different drivers over the years, whereas Figure 8(b) shows a box plot of the weights produced by statistics. The HAI weight average values from 2000 to 2020 were all negative, indicating a detrimental impact of human activity on UEQ in Shanghai. Precipitation and temperature as climatic elements can play varied positive and negative roles depending on the year. There is some degree of promotion of RSEI by the SQI and TCI. The impact values as seen in Figures 8(c) and 8(d), illustrate how much of an impact the components contribute to RSEI. The mean impact value of HAI weight is -0.142, which is much negatively greater than others, demonstrating that human activities have the greatest overall influence on the ecological environment. One of the main causes of the oscillations in the RSEI curve is due to climatic conditions, which have an impact on the relatively greater annual average variation. In contrast, the weights and impacts of non-climatic factors keep relatively stable.

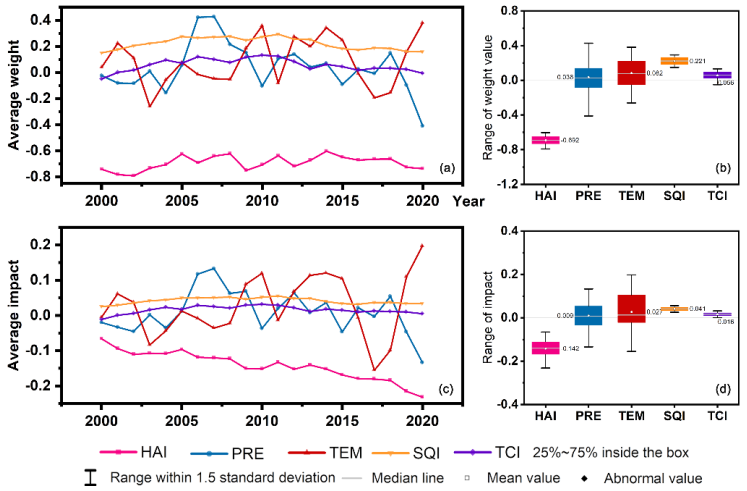

Fig 8. (a) Average weight change curve of drivers from 2000 to 2020; (b) Box graph of weights of drivers; (c) Average absolute weight change curve of drivers from 2000 to 2020; (d) Box graph of absolute weights of drivers

We employed a comparative analysis to examine the impacts of the drivers on the clusters and to identify the sources of the variations in evolving patterns. Figures 8(b) and 8(c) depict that, PRE displayed similar temporal effects on different classes, and numerous paired t-tests failed to reveal any statistically significant differences ($p>0.05$), which is a driving character also reflected by TEM. HAI, SQI, and TCI were the principal factors contributing to the variations between clusters. HAI exerted a more adverse influence on Classes I, II, and III, and this negative impact grew proportionately more rapidly over time. SQI exhibited a moderately beneficial impact on Class I, and the absence of surface soil in the core urban areas presented further challenges. It is noteworthy that Class VI, the most favorable zone for UEQ, was least negatively impacted by HAI. However, these areas had greater terrain demands, and the current terrain characteristics hindered the enhancement of local RSEI, impeding the improvement of UEQ.

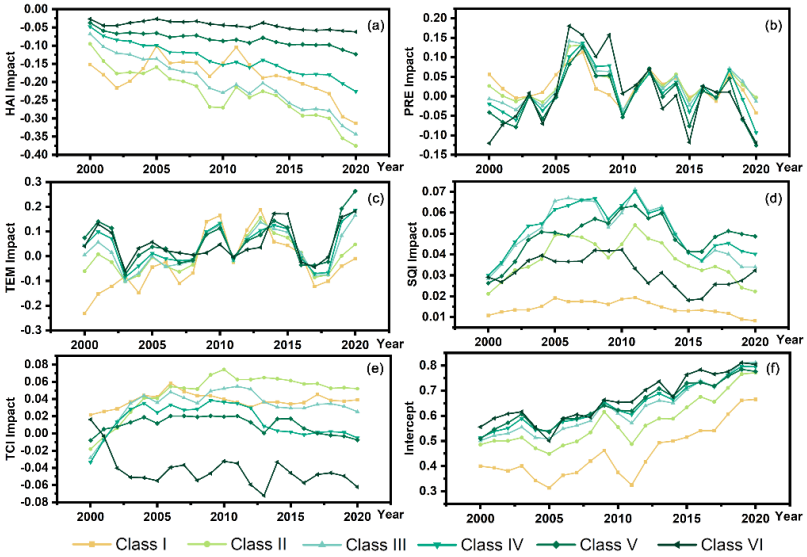

Fig 9. Time series curves of different drivers: (a) HAI; (b) PRE; (c) TEM; (d) SQI; (e) TCI; (f) Intercept value

As a reflection of the biome's ability to improve, the intercept value curves for each category (as demonstrated in Figure 8(f)) displayed a linear increase with a slope of approximately 0.0139 standard values per year (as listed in Table A5), indicating that the initial vegetation communities in Shanghai had inherent growth potential. A disturbance-free UEQ would therefore improve at a relatively constant rate. However, due to the interference from external factors, particularly anthropogenic activities, the overall RSEI growth rate decreased to 0.0075 standard values per year (as indicated in Table A5). The most significant impact was observed in Classes II and III, implying that external factors had the most detrimental effects on the ecosystems in these regions.

4 DISCUSSION

4.1 Attributions of ecological quality evolution

The principal finding of our investigation reveals an overall upward trend in the UEQ of Shanghai over the past two decades, particularly from 2005 to 2020. Similar trends have been observed in other areas of China recently (Li and Yang, 2022). However, the results for a megalopolis like Shanghai seem incomprehensible given that urban sprawl and population growth typically result in a decline in UEQ. Our study shows that the areas where UEQ has worsened are mainly limited to Class II regions; the vast majority have experienced an increase in UEQ at varying rates. Through driver analysis, we have discovered that the primary reason for the improvement is the natural ecosystem itself. The vegetation community of the ecological system has developed and enhanced the ecological environment (Li and Tian et al., 2023). The overall trend is positive since the overlap effects of other factors are insufficient to stifle this growing tendency.

The clustering results demonstrate that the distribution of UEQ evolutionary patterns conforms to a certain urban-rural gradient. We have corresponded each cluster in turn to the regional name of the urban structure to facilitate the summary of the driving mechanisms, as shown in Table A6. We then compared and summarized the discrepancies in the spatiotemporal driving characteristics and mechanisms among multiple factors, as shown in Table 1.

Table 1. Table of multifactorial spatiotemporal driving characteristics and mechanisms

Factor	Dimension	Driving characteristics and mechanisms
HAI	Spatial	The highly negative inhibitory effect gradually decreases along the urban-rural gradient.
	Temporal	Negative inhibition increased at different rates over time.
PRE	Spatial	Slight positive contribution, gradually decreasing along an urban-rural gradient.
	Temporal	Time series are highly volatile and the direction of action may change.
TEM	Spatial	Negative effect in the core urban area, and positive contribution in other areas.
	Temporal	Time series are highly volatile and the direction of action may change.
SQI	Spatial	Slighter positive contribution in the core urban area than in other places.
	Temporal	The overall time series are stable, but differ between regions, maintaining slight facilitative effects.
TCI	Spatial	Negative effect in the outer suburbs, and positive contribution in other areas.

	Temporal	The overall time series are stable but show a persistent negative impact in the outer suburbs
Intercept	Spatial	Gradually increasing along the urban-rural gradient.
	Temporal	The trend is consistent across regions, growing at similar rates, but differing at the numerical level.

It concludes that the combination of multiple factors affected the spatial differences in the trend. Furthermore, the mechanism behind the multifactorial discrepancies in the driving mechanisms can be explained in the following ways:

1) As with other research (Geng and Yu et al., 2022; Zhang and She et al., 2022), our study confirms that human activities continue to exert a significant influence on the environment and have substantially altered the process of urban ecosystem evolution. Out of all the drivers, human activities are the most damaging, relative to natural factors such as climate, topography, and soil. The central urban regions, their peripheries, and the urban-rural interface are more severely affected by human activities than suburban areas, and this impact is likely to worsen over time, leading to a future UEQ decline in more regions if it is not addressed (Li and Du et al., 2022).

2) Climate factors are not the principal cause of spatial differences, because the temporal heterogeneity of precipitation and temperature is much more robust than the spatial heterogeneity, and the differences between years are much more pronounced than those in space. There is no single positive or negative correlation between temperature or precipitation and RSEI; high or low temperatures as well as insufficient or excessive precipitation and could have negative impacts (Lafortezza and Sanesi, 2019). The impact of climate change has also long been a study challenge since many climate factors frequently have intricately intertwined consequences.

3) Favorable soil quality facilitates UEQ improvement, and it is noteworthy that the contribution of soil in the central urban regions is low. This may be because the extensive impermeable surfaces lead to the loss of surface soil. Therefore, it is necessary to emphasize the conservation of urban soils and strengthen the construction of urban green spaces and parks to better utilize the functional value of urban soils (Mexia and Vieira et al., 2018).

4) Topography only hinders a few locations, mostly the outer suburbs, and has little effect on many. The reason may be that these areas have a favorable ecological substrate and are more sensitive to terrain disturbance caused by development and construction. Megacities like Shanghai tend to possess flat topography, and spatially relatively small topographic differences do not render it a dominant driver.

5) The UEQ improvement function of biomes or vegetation communities themselves cannot be ignored, and their state is the main and fundamental driver of UEQ evolution (Chin and Kupfer, 2020). In urban ecosystems, vegetation communities, mainly in the form of parks and green areas, are irreplaceable for maintaining or improving the ecological environment of built-up areas (Evans and Falagán et al., 2022). At the same time, vegetation restoration or green space construction becomes an indispensable link in ecological planning and management (Johnson and Handel, 2016), providing valuable ecosystem services that in turn enhance human well-being.

Overall, due to the comprehensive influence of drivers, urban-rural spatial inequalities exist in the UEQ-improving trend in Shanghai. Therefore, in the future, differences in UEQ between urban and rural areas of large cities should be mitigated and regional ecological environments should be improved in an integrated and coordinated manner. How to develop targeted ecological management programs for regions with different evolution and driving patterns will become a practice issue worth exploring.

4.2 Model application considerations

In this study, we employed the GTWR, which is a reliable approach for investigating the influence of various factors and has shown better model-fitting performance than OLS and GWR, as previously reported in other research studies (Zhang and Sun et al., 2022). However, as a spatiotemporal model, the GTWR model has more hyperparameters and requires precise parameter adjustment, making it prone to overfitting. Therefore, caution must be exercised in selecting GTWR under all circumstances, and before constructing the model, strict tests for variable collinearity and spatiotemporal heterogeneity are required (Li and Chen et al., 2020). To thoroughly examine the impact of various aspects, we collected as much data as possible on the drivers. We used the VIF covariance test first and discovered the presence of several univariate VIFs above the threshold, as described in section 2.2. Due to the high spatial correlation among some variables, multicollinearity is such a problem addressed that a dimensionality reduction method like PCA is necessary.

Consistent with the RSEI construction, PCA employs the maximum principal component to retain the most information from multiple factors. Nevertheless, this method remains some limitations: 1) As a linear transformation dimensionality-reducing algorithm, PCA cannot account for complex nonlinear relationships that may exist among variables; 2) More than one principal component may be extracted (Hou and Wu et al., 2020), which reduces the explanatory ability of the maximum principal component.

In this study, we assumed that the core formula of GTWR maintained a linear form (Huang and Wu et al., 2010), implying establishing all explorations on a linear relationship. Therefore, linear dimensionality reduction using PCA was deemed appropriate. By properly categorizing variables, the main components of each kind into a single one, the resulting comprehensive index had sufficient load ratio and explanatory power. In section 2.3.2, we again used the VIF test and showed that the VIFs of all the composite indices were below the threshold and available for the GTWR.

Given that drivers may have complex nonlinear effects, a crucial scientific question for further research is to determine whether there are more suitable nonlinear dimensionality reduction models (Kostyuchenko, 2014) that can improve the performance to characterize UEQ and examine its drivers. In the future, deep learning models to uncover key drivers are a desperately awaited approach to better reveal the spatiotemporal driving mechanisms of UEQ.

4.3 Uncertainties and potential constraints

The following shortcomings of this study can be seen: 1) Due to a dearth of appropriate empirical research on various improved RSEI methods, we only utilized the classic RSEI model to represent UEQ. 2) There are still some deficiencies in the formation of the RSEI spatiotemporal sequences. We used Landsat 5 and 8 to construct

the RSEI, while the errors in calculating between the two sets of images should be objectively existent due to the differences in sensors. Most of the RSEI time series literature currently lacks a comparison and calibration of the results of the two calculations, which is also a limitation for our reference. 3) The time resolution is constrained. The time resolution of this study is one year. Advanced, the RSEI sequence can be accurate to the month or even more precisely. Climate factors may play a significant role in its seasonal variability, which is also an important direction for future research. 4) The predicted data used by SoilGrids lacks well-distributed points in some areas (Poggio and de Sousa et al., 2021). In addition, only picking a few soil property parameters as variables, and theoretically, more soil fertility factors should be considered and incorporated into the model. These issues may cause deviations in the soil quality index of the study area. Overall, future research should consider addressing these limitations to enhance accuracy and reliability.

5 CONCLUSION

In this study, we aimed to reveal multifactorial discrepancies in the spatiotemporal driving mechanisms on UEQ. By constructing long-term RSEI time series from 2000 to 2020, we investigated the spatiotemporal evolution and driving mechanisms of UEQ in Shanghai. We investigated how the UEQ is impacted by human activity, climate, geography, and soil elements using GTWR. In addition, we investigated the differences in the driving characteristics and mechanisms of multiple factors among different regions with the help of the K-Means clustering algorithm. The following are the primary conclusions:

1) UEQ marginally declined from 2000 to 2005 and significantly improved from 2005 to 2020 in Shanghai. The main driving force of UEQ improvement was the self-functional development of vegetation communities, which was also influenced and disturbed by a combination of abiotic factors including human activities, climate, soil, and topography.

2) The clustering of UEQ evolution in Shanghai is consistent with a certain urban-rural gradient. Multiple factors' driving roles and characteristics differ in different clustering areas, forming a differentiated driving mechanism that jointly influences the trajectory of UEQ spatial and temporal evolution.

3) Human activities play the largest negative inhibitory role. The direction and degree of influence of each of the other factors vary among regions or along the urban-rural gradient. Climatic factors show highly fluctuating temporal serial characteristics. Biome factors such as vegetation maintain a specific uprising rate. The time series of each of the other factors is relatively stable but varies among regions.

Our conclusions further emphasize that green space and vegetation play an important role in improving UEQ, and provide an opportunity for Shanghai and other regions to improve the environment. They also verify the differential effects of human activities and climate change on regional UEQ and deepened the understanding of multifactorial driving mechanisms. These findings can provide references for environmental observations, targeted ecological management, and planning in Shanghai and other urban areas, promoting sustainable development.

REFERENCES

[1] Arfanuzzaman, M. and B. Dahiya (2019). "Sustainable urbanization in Southeast Asia and beyond: Challenges of population growth, land use change, and environmental health." Growth and change **50** (2): 725-744.

[2] Ariken, M. and F. Zhang, et al. (2020). "Coupling coordination analysis of urbanization and eco-environment in Yanqi Basin based on multi-source remote sensing data." Ecological Indicators **114**: 106331.

[3] Bo, Y. and X. Li, et al. (2022). "Three Decades of Gross Primary Production (GPP) in China: Variations, Trends, Attributions, and Prediction Inferred from Multiple Datasets and Time Series Modeling." Remote Sensing **14** (11).

[4] Braun, D. and R. de Jong, et al. (2019). "Ecosystem service change caused by climatological and non-climatological drivers: a Swiss case study." Ecol Appl **29** (4): e01901.

[5] Chen, A. and X. Yang, et al. (2022). "Dynamic of land use, landscape, and their impact on ecological quality in the northern sand-prevention belt of China." Journal of Environmental Management **317**: 115351.

[6] Chen, J. and M. Gao, et al. (2022). "Global 1 km x 1 km gridded revised real gross domestic product and electricity consumption during 1992-2019 based on calibrated nighttime light data." Sci Data **9** (1): 202.

[7] Chen, Z. and B. Yu, et al. (2021). "An extended time series (2000–2018) of global NPP-VIIRS-like nighttime light data from a cross-sensor calibration." Earth system science data **13** (3): 889-906.

[8] Cheng, J. and S. Dai, et al. (2016). "Spatiotemporal heterogeneity of industrial pollution in China." China Economic Review **40**: 179-191.

[9] Cheng, Y. and H. Liu, et al. (2022). "Human Activity Intensity and Its Spatial-Temporal Evolution in China's Border Areas." LAND **11** (7).

[10] Chin, E. Y. and J. A. Kupfer (2020). "Identification of environmental drivers in urban greenway communities." Urban forestry & urban greening **47**: 126549.

[11] Dogan, E. and R. Ulucak, et al. (2020). "The use of ecological footprint in estimating the Environmental Kuznets Curve hypothesis for BRICST by considering cross-section dependence and heterogeneity." Sci Total Environ **723**: 138063.

[12] Evans, D. L. and N. Falagán, et al. (2022). "Ecosystem service delivery by urban agriculture and green infrastructure – a systematic review." Ecosystem Services **54**: 101405.

[13] Frédéric, G. and C. Jean-Marc (2018). "Relationships between human activity and biodiversity in Europe at the national scale: Spatial density of human activity as a core driver of biodiversity erosion." Ecological Indicators **90**.

[14] Geng, J. and K. Yu, et al. (2022). "Analysis of Spatiotemporal Variation and Drivers of Ecological Quality in Fuzhou Based on RSEI." Remote sensing (Basel, Switzerland) **14** (19): 4900.

[15] Guo, B. and Y. Fang, et al. (2020). "Monitoring the effects of land consolidation on the ecological environmental quality based on remote sensing: A case study of Chaohu Lake Basin, China." Land Use Policy **95**: 104569.

[16] Harris, I. and T. J. Osborn, et al. (2020). "Version 4 of the CRU TS monthly high-resolution gridded multivariate climate dataset." Scientific data **7** (1): 109-109.

[17] Hou, L. and F. Wu, et al. (2020). "The spatial characteristics and relationships between landscape pattern and ecosystem service value along an urban-rural gradient in Xi'an city, China." Ecological Indicators **108**: 105720.

[18] Hu, J. and J. Zhang, et al. (2022). "Exploring the spatial and temporal driving mechanisms of landscape patterns on habitat quality in a city undergoing rapid urbanization based on GTWR and MGWR: The case of Nanjing, China."

Ecological indicators **143**: 109333.

[19] Hu, X. and H. Xu (2018). "A new remote sensing index for assessing the spatial heterogeneity in urban ecological quality: A case from Fuzhou City, China." Ecological indicators **89**: 11-21.

[20] Huang, B. and B. Wu, et al. (2010). "Geographically and temporally weighted regression for modeling spatio-temporal variation in house prices." INTERNATIONAL JOURNAL OF GEOGRAPHICAL INFORMATION SCIENCE **24** (3): 383-401.

[21] Ji, J. and S. Wang, et al. (2020). "Spatiotemporal Change and Landscape Pattern Variation of Eco-Environmental Quality in Jing-Jin-Ji Urban Agglomeration From 2001 to 2015." IEEE access **8**: 125534-125548.

[22] Jiang, F. and Y. Zhang, et al. (2021). "Research on remote sensing ecological environmental assessment method optimized by regional scale." Environ Sci Pollut Res Int **28** (48): 68174-68187.

[23] Jing, Y. and F. Zhang, et al. (2020). "Assessment of spatial and temporal variation of ecological environment quality in Ebinur Lake Wetland National Nature Reserve, Xinjiang, China." Ecological Indicators **110**: 105874.

[24] Johnson, L. R. and S. N. Handel (2016). "Restoration treatments in urban park forests drive long-term changes in vegetation trajectories." Ecol Appl **26** (3): 940-56.

[25] Khan, I. and F. Hou, et al. (2021). "The impact of natural resources, energy consumption, and population growth on environmental quality: Fresh evidence from the United States of America." The Science of the total environment **754**: 142222-142222.

[26] Knight, S. J. and C. J. McClean, et al. (2022). "The importance of ecological quality of public green and blue spaces for subjective well-being." Landscape and Urban Planning **226**: 104510.

[27] Komugabe-Dixson, A. F. and N. S. E. de Ville, et al. (2019). "Environmental change, urbanisation, and socio-ecological resilience in the Pacific: Community narratives from Port Vila, Vanuatu." Ecosystem Services **39**: 100973.

[28] Kostyuchenko, Y. V. (2014). Geostatistics and Remote Sensing for Extremes Forecasting and Disaster Risk Multiscale Analysis. Cham, Springer International Publishing: 439-458.

[29] Kun, Y. and Y. Zhenyu, et al. (2019). "Spatial-temporal variation of lake surface water temperature and its driving factors in Yunnan-Guizhou Plateau." Water resources research **55** (6): 4688-4703.

[30] Lafortezza, R. and G. Sanesi (2019). "Nature-based solutions: Settling the issue of sustainable urbanization." Environ Res **172**: 394-398.

[31] Li, D. and W. Yang (2022). "The regional difference, dynamic evolution, and multidimensional inequality of China's ecological environment quality from the concept of ecological resilience." Environmental science and pollution research international.

[32] Li, G. and W. Chen, et al. (2020). "Prediction of AOD data by geographical and temporal weighted regression with nonlinear principal component analysis." Arabian journal of geosciences **13** (17).

[33] Li, J. and M. Bi, et al. (2022). "Investigating the Impacts of Urbanization on Vegetation Net Primary Productivity: A Case Study of Chengdu–Chongqing Urban Agglomeration from the Perspective of Townships." Land (Basel) **11** (11): 2077.

[34] Li, N. and J. Wang (2022). "Comprehensive Eco-Environment Quality Index Model with Spatiotemporal Characteristics." Sensors (Basel) **22** (24).

[35] Li, X. Y. and L. Du, et al. (2022). "Effects of Human Activities on Urban Vegetation: Explorative Analysis of Spatial Characteristics and Potential Impact Factors." REMOTE SENSING **14** (13).

[36] Li, Y. and H. Tian, et al. (2023). "Detection of spatiotemporal changes in ecological quality in the Chinese mainland: Trends and attributes." Science of The Total Environment **884**: 163791.

[37] Lyu, R. and K. C. Clarke, et al. (2019). "Spatial correlations among ecosystem services and their socio-ecological driving factors: A case study in the city belt along the Yellow River in Ningxia, China." Applied geography (Sevenoaks) **108**: 64-73.

[38] Mexia, T. and J. Vieira, et al. (2018). "Ecosystem services: Urban parks under a magnifying glass." Environmental Research **160**: 469-478.

[39] Nichol, J. (2005). "Remote sensing of urban heat islands by day and night." PHOTOGRAMMETRIC ENGINEERING AND REMOTE SENSING **71** (5): 613-621.

[40] Paul, G. C. and S. Saha, et al. (2020). "Assessing the soil quality of Bansloi river basin, eastern India using soil-quality indices (SQIs) and Random Forest machine learning technique." Ecological indicators **118**: 106804.

[41] Poggio, L. and L. M. de Sousa, et al. (2021). "SoilGrids 2.0: producing soil information for the globe with quantified spatial uncertainty." SOIL **7** (1): 217-240.

[42] Ren, H. and Y. Shang, et al. (2020). "Measuring the spatiotemporal variations of vegetation net primary productivity in Inner Mongolia using spatial autocorrelation." Ecological Indicators **112**: 106108.

[43] Sun, C. and J. Li, et al. (2022). "Ecological quality assessment and monitoring using a time-series remote sensing-based ecological index (ts-RSEI)." GIScience & Remote Sensing **59** (1).

[44] Suominen, T. (2018). "Applying MERIS time series and dynamic time warping for delineating areas with similar temporal behaviour in the northern Baltic Sea." Ecological indicators **95**: 794-804.

[45] Tang, W. and S. Liu, et al. (2023). "Evolution and improvement options of ecological environmental quality in the world's largest emerging urban green heart as revealed by a new assessment framework." The Science of the total environment **858**: 159715.

[46] Toth, Z. and M. Dombos, et al. (2023). "Urban soil quality deteriorates even with low heavy metal levels: An arthropod-based multi-indices approach." Ecol Appl **33** (4): e2848.

[47] Viana-Soto, A. and I. Aguado, et al. (2020). "Identifying Post-Fire Recovery Trajectories and Driving Factors Using Landsat Time Series in Fire-Prone Mediterranean Pine Forests." Remote sensing (Basel, Switzerland) **12** (9): 1499.

[48] Wang, J. and X. Ma, et al. (2019). "Improved K-means Clustering k-Value Selection Algorithm." Computer Engineering and Applications **55** (8): 27-33.

[49] Wang, M. and X. Fu, et al. (2023). "Assessing urban flooding risk in response to climate change and urbanization based on shared socio-economic pathways." Sci Total Environ **880**: 163470.

[50] Wang, S. and Z. Liu, et al. (2021). "Factors influencing ecosystem services in the Pearl River Delta, China: Spatiotemporal differentiation and varying importance." Resources, conservation and recycling **168**: 105477.

[51] Wang, Z. and L. Liang, et al. (2019). "Spatiotemporal differentiation and the factors influencing urbanization and ecological environment synergistic effects within the Beijing-Tianjin-Hebei urban agglomeration." J Environ Manage **243**: 227-239.

[52] Wang, Z. and T. Chen, et al. (2023). "RSEIFE: A new remote sensing ecological index for simulating the land surface eco-environment." Journal of Environmental Management **326**: 116851.

[53] Wei, Q. and L. Zhang, et al. (2019). "Global and Geographically and Temporally Weighted Regression Models for Modeling PM(2.5) in Heilongjiang, China from 2015 to 2018." Int J Environ Res Public Health **16** (24).

[54] Xu, H. Q. and C. Q. Li, et al. (2022). "Is the z-score standardized RSEI suitable for time-series ecological change detection? Comment on Zheng et al. (2022)." SCIENCE OF THE TOTAL ENVIRONMENT **853**.

[55] Xu, H. Q. and Y. F. Wang, et al. (2019). "Detecting Ecological Changes with a Remote Sensing Based Ecological Index (RSEI) Produced Time Series and Change Vector Analysis." REMOTE SENSING **11** (20).

[56] Yang, J. and X. Huang (2021). "The 30 m annual land cover dataset and its dynamics in China from 1990 to 2019." Earth system science data **13** (8): 3907-3925.

[57] Yang, Z. and J. Tian, et al. (2021). "Spatio-temporal pattern and evolution trend of ecological environment quality in the Yellow River Basin." Acta Ecologica Sinica **41** (19): 7627-7636.

[58] Yu, Y. and Q. Shao, et al. (2018). "Regionalization study of maximum daily temperature based on grid data by an objective hybrid clustering approach." Journal of Hydrology **564**: 149-163.

[59] Yuan, B. and L. Fu, et al. (2021). "Spatiotemporal change detection of ecological quality and the associated affecting factors in Dongting Lake Basin, based on RSEI." Journal of cleaner production **302**: 126995.

[60] Zhang, S. and P. Yang, et al. (2021). "Research and Analysis of Ecological Environment Quality in the Middle Reaches of the Yangtze River Basin between 2000 and 2019." Remote Sensing **13** (21).

[61] Zhang, X. and Y. Sun, et al. (2022). "Research on the Temporal and Spatial Distributions of Standing Wood Carbon Storage Based on Remote Sensing Images and Local Models." Forests **13** (2): 346.

[62] Zhang, Y. and J. She, et al. (2022). "Spatio-temporal evolution and driving factors of eco-environmental quality based on RSEI in Chang-Zhu-Tan metropolitan circle, central China." Ecological Indicators **144**: 109436.

[63] Zhang, Z. and Y. Fan, et al. (2023). "Wetland ecological index and assessment of spatial-temporal changes of wetland ecological integrity." Sci Total Environ **862**: 160741.

[64] Zhang, Z. and Z. Cai, et al. (2022). "Ecological environmental quality assessment of Chinese estuarine wetlands during 2000–2020 based on a remote sensing ecological index." Frontiers in Marine Science **9**.

[65] Zheng, Z. and Z. Wu, et al. (2022). "Instability of remote sensing based ecological index (RSEI) and its improvement for time series analysis." The Science of the total environment **814**: 152595-152595.

[66] Zou, C. and J. Zhu, et al. (2022). "Coupling coordination and spatiotemporal heterogeneity between urbanization and ecological environment in Shaanxi Province, China." Ecological indicators **141**: 109152.